Delft University of Technology

Uncertainty quantification for solar sails in the near-Earth environment

Garcia Bonilla, J.; Carzana, L.; Heiligers, M.J.

Important note
To cite this publication, please use the final published version (if applicable).
Please check the document version above.

Uncertainty quantification for solar sails in the near-Earth environment

Juan GARCIA-BONILLA[1,*], Livio CARZANA[1], Jeannette HEILIGERS[1]

[a] Faculty of Aerospace Engineering, Delft University of Technology, Delft, the Netherlands

Abstract

This paper addresses the significance of uncertainty quantification in solar-sail missions, focusing on the uncertainties associated with the sail's optical coefficients, structural deformation, and attitude profiles for missions in the Earth environment. Due to the relatively low technological maturity of solar-sailing systems, understanding and quantifying uncertainties is crucial for mission success and reliability. This paper employs the Gauss von Mises method for uncertainty propagation and stochastic integration of Ornstein-Uhlenbeck processes, which proved to be robust methodologies for quantifying and modelling uncertainties. The results show a significant impact of uncertainties in the optical coefficients on mission performance, exemplified by a 3-σ uncertainty of 7.5% on the increase in semi-major axis achieved during orbit raising maneuvers using the coefficient uncertainties of the NEA Scout mission. As another example, the analysis on attitude uncertainty demonstrates a 3% lower mean performance in terms of altitude gain compared to ideal control profiles. The research furthermore underscores the effectiveness of the Gauss von Mises method, offering great computational efficiency compared to Monte Carlo simulations. These findings highlight the necessity of considering uncertainty in solar-sail missions and provide valuable insights for improved mission planning, risk assessment, and decision-making.

Keywords: Solar sailing, near-Earth environment, Uncertainty quantification, Gauss von Mises, Stochastic Differential Equation

1. Introduction

Solar sailing has revolutionized space exploration by harnessing the pressure of sunlight to propel spacecraft, offering increased maneuverability and reduced fuel requirements compared to conventional propulsion systems [1]. However, the success and reliability of solar-sail missions depend on a comprehensive understanding and quantification of inherent uncertainties, considering the relatively low technological maturity of these systems.

Quantifying uncertainties is essential for risk mitigation, mission optimization, and informed decision-making. Moreover, it enables the development of robust control strategies capable of addressing unexpected variations and disturbances during operation.

Recent publications have highlighted the significance of uncertainty quantification in solar-sail missions. For instance, Yamaguchi et al. discussed the challenges of developing precise solar-sail force models on the ground and proposed estimation strategies based on orbital data [2]. Eldad et al. developed robust attitude control algorithms that account for uncertainties in sail deformation, moment of inertia, and effective reflectivity [3]. Similarly, Nicolai et al. employed a polynomial chaos procedure to investigate the impact of uncertain solar-sail optical coefficients and solar irradiance on heliocentric trajectories [4]. Oguri et al. explored robust trajectory design for the NEA Scout mission, considering uncertainties in solar pressure acceleration [5].

This paper, on the other hand, focuses on the uncertainties associated with the solar-sail optical coefficients, structural deformation, and non-ideal attitude profiles for missions in the Earth environment. Quantifying optical coefficients, which are influenced by complex phenomena like wrinkling, presents challenges; extensive testing campaigns for the NEA Scout solar-sail revealed significant uncertainties [6]. Modeling sail deformation, on the other hand, remains uncertain due to the lack of experimental data. Finally, mission data from, for example the LightSail-2 mission, has demonstrated the difficulty of adhering to predefined control profiles, resulting in notable attitude deviations [7].

As such, this paper provides the first insights into the effect of uncertainty in the solar-sail optical coefficients,

---

*Corresponding author, juan@garciabonilla.com

structural deformation, and attitude control in the Earth environment. Moreover, it does so by utilizing novel techniques in the field, such as the computationally-inexpensive Gauss von Mises uncertainty propagation method or the use of Ornstein-Uhlenbeck processes to model attitude uncertainty [8][9].

While the problem of uncertainty quantification is applicable to various scenarios and sources of uncertainty, we delve into a specific case study to shed light on the broader issue of uncertainty propagation for solar sails within the Earth environment. The selected case study draws inspiration from the ACS3 mission, utilizing its sail loading parameter and initial Dawn-Dusk Sun-Synchronous Orbit [10].

Following this brief introduction, the paper proceeds with two sections on the methodology employed, introducing the relevant dynamical models, studied uncertainties, and uncertainty propagation methods. Subsequently, the case study is further discussed and selected results of the uncertainty analysis are presented, followed by a concise conclusion.

2. Dynamical models

In this section, the solar-sail dynamical model and attitude control strategy employed in the remainder of the paper are presented.

2.1. Solar sail dynamics

The dynamics of the solar sail are expressed in the J2000 Earth-centered inertial reference frame through the following equation of motion:

$$\frac{d\mathbf{v}}{dt} = \mathbf{a}_{\text{total}} = \frac{\text{GM}_{\text{E}}}{r_{E\to s}^3}\vec{r}_{E\to s} + \mathbf{a}_{\text{J2}} + \mathbf{a}_{\text{SRP}} + \mathbf{a}_{\text{aero}} \quad (1)$$

where $\text{GM}_{\text{E}} = 398600.4415 \text{km}^3/\text{s}^2$ is the Earth's gravitational parameter [11], $\vec{r}_{E\to s}$ is the position vector of the sail, $\mathbf{a}_{\text{J2}}$ is the acceleration due the J_2 coefficient perturbation, $\mathbf{a}_{\text{SRP}}$ is the Solar Radiation Pressure (SRP) acceleration, and $\mathbf{a}_{\text{aero}}$ is the acceleration due to aerodynamic forces. For this first investigation into uncertainty quantification in the solar-sail near-Earth orbital dynamics, smaller perturbations including planetary radiation pressure, third-body effects, and higher-order Earth gravity terms are ignored.

The J_2 acceleration, $\mathbf{a}_{\text{J2}}$, is modeled as per Eq. 20.6 in Ref. [11], taking values for the reference radius and J_2 as published in the GGM03 model [12].

The SRP acceleration, $\mathbf{a}_{\text{SRP}}$, is modelled through the Generalized Sail Model (GSM) developed by Rios-Reyes and Scheeres [13]. This method can compute the SRP force of non-ideal, non-flat solar sails at low computational costs under the following assumptions: the shape is fixed over time, the same side of the sail is always illuminated, and there is no self-shadowing.
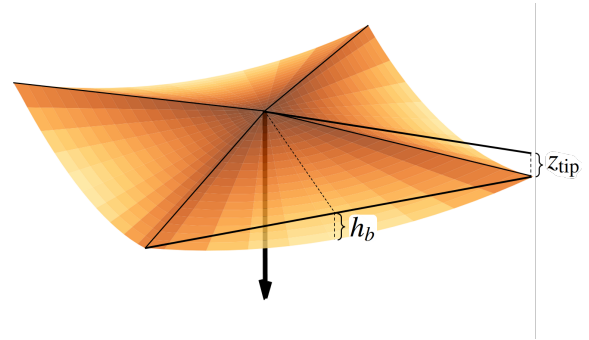

Figure 1: Four-quadrant, square solar-sail model with billowing and boom bending. Lighter colors are further apart from the nominal plane of the sail.

In this paper, the GSM is used to model a square-shaped solar sail subject to constant deformations. More specifically, the sail is modeled as a four-quadrant billowed surface with bent linear booms along the diagonals, as displayed in Fig. 1.

The sail billowing and bending are characterized by two parameters, the maximum billow height ($h_b > 0$) and the boom tip displacement ($z_{\text{tip}} > 0$), see Fig. 1. The maximum billow height represents the largest distance between the sail surface and the line connecting the boom tips. On the other hand, the boom tip displacement measures the distance between the sail nominal plane and the boom tips, assuming that the boom deflection is linear from root to tip.

Apart from the sail shape parameters, the SRP acceleration also depends on the sail's optical properties, which are described by the reflectivity ρ, specularity s, the Lambertian coefficients of the front and back sides of the sail, B_f and B_b, respectively, and emissivity of the front and back sides of the sail, ε_f and ε_b, respectively. For further insights into these optical coefficients, the reader is referred to Ref. [1].

The aerodynamic acceleration, $\mathbf{a}_{\text{aero}}$, is obtained by assuming a non-rotating flat sail in hyperthermal free-molecular flow. This model was considered because, given the low angular rate of the sail compared to its velocity, the non-rotating sail assumption is justified. Moreover, given that aerodynamic forces are an order of magnitude weaker than solar radiation pressure, the sail's deformation is considered negligible when computing the aerodynamic force.

Furthermore, the assumption of a hyperthermal free-molecular flow has been used often in the literature to

describe the dynamics of air particles relative to a sail-craft in Earth orbit [14][15]. It assumes the random thermal motion of the air molecules to be much slower than the velocity of the spacecraft and is valid for large Knudsen numbers, meaning that the fluid-continuum assumption of the air is no longer applicable [16].

Section 2.3.2 of Ref. [16] contains the relevant equations to compute the aerodynamic forces, using the following parameters as defined in this reference: $V_w/V = 0.05$, and $\sigma_t = \sigma_n = 0.8$. Moreover, this paper assumes an exponential atmosphere with reference radius $R_E = 6378.1363$ km, scale height $H = 7.02503$ km, and reference density $\rho_0 = 1.225$ kg/m^3.

2.2. Attitude control

Both the SRP acceleration and aerodynamic forces strongly depend on the attitude of the sail, and thus attitude control is the primary control strategy for solar-sailcraft. This paper considers ideal locally optimal steering laws for planet-centered solar-sailing, as described by Macdonald and McInnes [17][18].

3. Uncertainty

This section encompasses the modeling of uncertainties, their propagation, and their impact on a specific figure of merit.

3.1. Constant random value uncertainties

This study considers uncertainty due to unknown sail deformation parameters (h_b, z_{tip}) and optical coefficients (ρ, s, B_f, B_b, ε_f, ε_b). These values are assumed to be normally distributed random variables that remain constant during propagation.

The uncertainty in these input parameters is propagated into the uncertainty in some figure of merit through Monte Carlo (MC) simulations and the Gauss von Mises (GVM) method [8]. The GVM method is an uncertainty propagation method that requires only between 10 to 20 sample propagations to produce estimates of the figure of merit distribution, compared to the thousands of propagations that the MC method might require to do the same.

This paper presents results obtained using both the GVM and MC methods to demonstrate whether the GVM method is capable of accurately capturing output distributions at the benefit of being orders of magnitude faster than MC. As such, the MC method serves as the validation mechanism for the results shown in this paper.

3.2. Stochastic process uncertainties

In order to consider uncertainties in the attitude control of the sail over the mission profile, some simulations presented in this paper also consider an attitude offset with respect to the nominal attitude profile (i.e., the ideal locally optimal steering laws). This attitude offset is used to represent more realistic attitude profiles, as found in solar-sail missions with imperfect GNC systems [7].
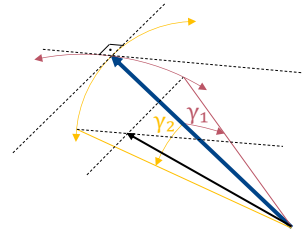

Figure 2: Sketch of the offset sail normal (shown as a black arrow) and the reference sail normal (blue arrow). The angular offsets γ_1 and γ_2 are shown in red and yellow respectively.

This attitude offset is defined by two parameters (γ_1 and γ_2) which represent angular displacements along two arbitrarily chosen perpendicular directions with respect to the sail normal, see Fig. 2.

The angular offsets γ_1 and γ_2 vary randomly in time and are modelled as independent and identical stochastic Ornstein-Uhlenbeck processes [9]. These can be regarded as variations of "random walks" (Wiener) processes, in which there is a tendency to drift towards the mean value $\gamma_1 = \gamma_2 = 0$. These processes are defined by the following Stochastic Differential Equation [9]:

$$d\gamma_i = -\theta\gamma_i dt + \sigma d\beta(t) \tag{2}$$

where θ and σ are the characteristic parameters of the Ornstein-Uhlenbeck process, and $\beta(t)$ is a one dimensional Brownian motion process. An important characteristic of these processes is that they have a bounded standard deviation, given by $\sigma_{st} = \sigma/\sqrt{2\theta}$.

Because the angular offsets γ_1 and γ_2 impact the direction of the sail normal and, therefore, the entire solar-sail dynamics, Eqs. 1 and 2 are coupled. Consequently, they ought to be propagated in parallel:

$$d\begin{bmatrix} \mathbf{v} \\ \gamma_1 \\ \gamma_2 \end{bmatrix} = \begin{bmatrix} \mathbf{a}_{total} \\ -\theta\gamma_1 \\ -\theta\gamma_2 \end{bmatrix} dt + \begin{bmatrix} \mathbf{0} \\ \sigma_{st}\sqrt{2\theta} \\ \sigma_{st}\sqrt{2\theta} \end{bmatrix} d\beta(t) \tag{3}$$

Moreover, due to the presence of Stochastic Differential Equations in the above system of equations, propagation must be performed using a stochastic integrator. In this paper, the weak third-order, additive-noise

stochastic integrator by Debrabant is used with a time step of 10 seconds [19].

Uncertainty due to stochastic processes cannot be modelled through the GVM method, as this method is only apt for modelling random but constant variables. Thus, only the MC method is used to generate results for the uncertainty due to an attitude offset.

4. Results

This section introduces the test case used to evaluate and validate the methodology presented in the previous sections, as well as to obtain insights into the wider problem of uncertainty in solar-sail missions in the Earth environment. Subsequently, the results of the uncertainty propagation analysis due to the constant random value uncertainties (deformation and optical parameters) and stochastic process uncertainties (attitude offset) are presented.

4.1. Test case

The following test case is inspired by the ACS3 mission, considering a similar initial Dawn-Dusk Sun-Synchronous orbit $[a, e, i, \Omega, \omega, f]_0 = [7071 \text{ km}, 0, 98.16 \text{ deg}, 0 \text{ deg}, 90 \text{ deg}, 0 \text{ deg}]$ [10]. A locally optimal steering law for the sail is employed that maximizes the rate of change of the semi-major axis (SMA) [17][18].
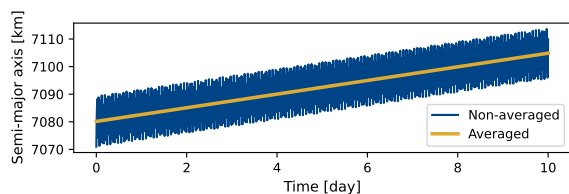

Figure 3: Evolution of the semi-major axis of the nominal test case (without uncertainties).

Figure 3 displays the increase in SMA for the nominal test case. The inclusion of J_2 perturbations introduces a strong oscillatory behaviour, as seen in the "Non-averaged" line. Because this hampers analysis, a locally averaged SMA is considered, which removes these oscillations and provides a more accurate depiction of the SMA increase due to the solar sail. Note that the averaged SMA increase is linear.

In this paper, the figure of merit for analysis is the SMA increase after some days of orbit raising maneuvers (Δa). This value is defined as the difference between the averaged SMA at some time t and the same quantity at time t_0. Finally, note that whenever reference values of the SMA increase Δa_{ref} are used, these values

refer to the SMA gain obtained in the nominal case (as presented in Fig. 3).

Table 1: Nominal value and standard deviations of the input uncertainties considered in the studied test case. Note that $\sigma_2 = 2\sigma_1$.

	Nominal (Mean)	σ_1	σ_2
σ_{load} [kg/m^2]	0.20266	-	-
l [m]	7.0	-	-
ρ [-]	0.910	0.005	0.010
s [-]	0.890	0.045	0.090
B_f [-]	0.79	0.05	0.10
B_b [-]	0.67	0.05	0.10
ε_f [-]	0.025	0.005	0.010
ε_b [-]	0.270	0.005	0.010
h_b [m]	0.100	0.025	0.0430
z_{tip} [m]	0.3500	0.0875	0.175

Table 1 shows the the nominal parameters that define the solar sail considered in this paper, as well as the associated uncertainties that will be studied in Section 4.2.1. The sail's loading parameter, σ_{load}, which is the ratio between the sail's mass to its area, and its boom length, l, are obtained from data relevant to the Advanced Composite Solar Sail (ACS3)[1]. The optical coefficient data is obtained from the NEA Scout solar sail model [6]. Finally, deformation parameters have been chosen based on the limited data presented by Greschik and Mikulas, and their standard deviations were chosen conservatively large: a fourth and half of the nominal value for σ_1 and σ_2 respectively [20].

Propagation is done for either 1, 5, or 10 days, depending on the analysis. 10,000 samples are used for every Monte Carlo simulation presented in this paper. When no stochastic process have to be integrated, an 8th order Runge-Kutta integrator with 64 seconds time step is used.

4.2. Constant random value uncertainties

This section covers selected results from an analysis on the effect of constant random value uncertainties on the figure of merit uncertainty. First, different uncertainties are studied independently. Subsequently, a detailed analysis of the uncertainty due to specularity is presented. Finally, a coupled analysis of all uncertainties is discussed.

4.2.1. Uncertainty due to uncoupled uncertainties

This section presents the uncertainty in SMA increase after 1 day of maneuvers due the input uncertainties displayed in Table 1. Each source of uncertainty is studied

---

[1]Data taken from communication with the ACS3 team at NASA's Langley Research Center.

independently, and two standard deviations are considered for each input uncertainty (σ_1 and σ_2).

Table 2: Normalized semi-major axis gain standard deviation obtained after 1 day of maneuvers for different input uncertainties and according to the Monte Carlo and Gauss von Mises simulations. Columns labeled "Diff" show the difference between the Gauss von Mises and Monte Carlo results. Values for σ_1 and σ_2 are provided in Table 1.

	$\sigma_{\Delta a}/\Delta a_{\text{ref}}$ [%]					
	σ_1			σ_2		
	MC	GVM	Diff	MC	GVM	Diff
ρ	0.79	0.79	-0.001	1.56	1.57	0.010
s	2.55	2.57	0.019	4.25	4.44	0.190
B_f	0.41	0.41	-0.003	0.78	0.82	0.040
B_b	0.31	0.31	0.001	0.62	0.63	0.004
ε_f	0.16	0.16	0.001	0.31	0.31	0.007
ε_b	0.01	0.02	0.005	0.03	0.03	0.003
h_b	0.04	0.05	0.002	0.09	0.11	0.028
z_{tip}	0.20	0.21	0.002	0.46	0.46	0.004

Table 2 shows the ratio of the standard deviation and reference value of the SMA gain caused by each input uncertainty, as obtained from the Monte Carlo and Gauss von Mises methods. A value of 2.5% in this ratio, for example, means that for a nominal SMA gain of 10 km, the uncertain SMA increase would have a 750 m 3σ uncertainty.

It is apparent that the GVM method can provide accurate estimates of the true standard deviations (obtained from MC simulations) independently of the input uncertainty and its magnitude, at a computational cost that is orders of magnitude lower than Monte Carlo simulations. In most cases, the GVM method produces slightly larger (more conservative) standard deviations than MC.

Table 2 additionally provides a clear hierarchy of the most impactful input uncertainties. The uncertainty in specularity has the strongest effect, followed by the uncertainty in reflectivity. On the other hand, the uncertainty due to the emissivity coefficients and the deformation parameters is considerably smaller. As such, it is of interest to evaluate whether the effects of the latter uncertainties are negligible compared to the effects of the former in a coupled analysis, which is presented in Section 4.2.3.

4.2.2. Detailed analysis of uncertain specularity

The previous section provided a first order characterization of the impact of every input uncertainty on the figure of merit. This section, in turn, provides a deeper exploration of the figure of merit distribution due to a single uncertain input: the specularity.

Figure 4 shows the distribution of the normalized relative SMA gain with respect to the reference SMA gain
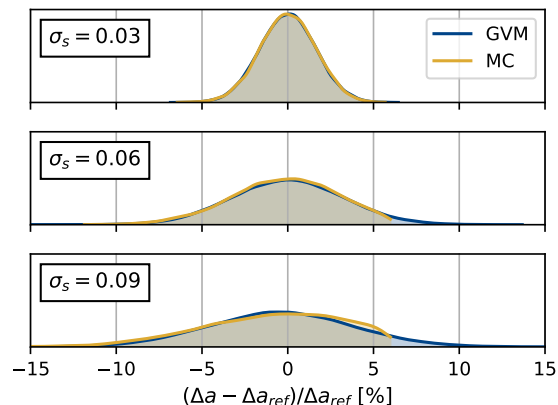

Figure 4: Distribution of the semi-major axis increase after 10 days of maneuvers according to Monte Carlo and Gauss von Mises simulations. Results are presented for three different specularity standard deviations, σ_s.

after 10 days of maneuvers for three specularity standard deviations, σ_s.

The normalized relative SMA gain measures how much the uncertain case underperforms or overperforms with respect to the nominal case. For instance, a -5% relative SMA gain when the nominal gain is 10 km means that the uncertain case obtained a SMA gain of only 9.5 km. Positive relative SMA gains, on the other hand, produce SMA gains above the nominal case, which can happen for specularities that are higher than the nominal specularity, and thus are closer to an ideal solar sail and are thus more performant.

Figure 4 also demonstrates that the SMA gain distribution closely follows a normal distribution. Moreover, the Gauss von Mises method is capable of accurately capturing the same behaviour as the more computationally expensive Monte Carlo simulations, independently of the standard deviation of the specularity.

Additionally, Figure 4 reveals that the results for the GVM method extend beyond those for the MC simulation for positive relative SMA gains. This means that the truncation behaviour that the MC method exhibits is not captured by the GVM method, which showcases how the latter method can miss certain details about the real distribution.

Figure 5 shows how the SMA distribution remains normal during propagation, with the results from the GVM method once again closely agreeing with the results from MC simulations. Interestingly, the spread of the distributions remains similar for the three times presented. This suggests that the standard deviation of the SMA gain $\sigma_{\Delta a}$ grows like the reference value Δa_{ref}: linearly.
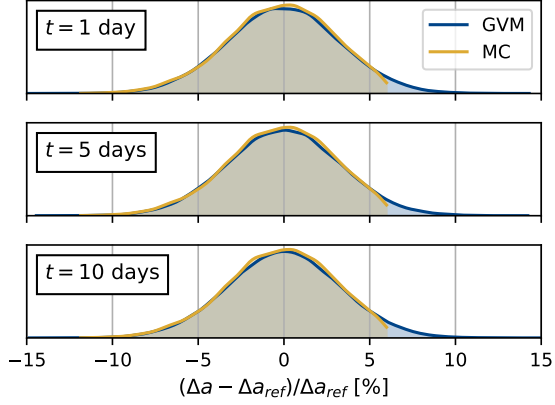
Figure 5: Distribution of the semi-major axis increase due to a specularity standard deviation of $\sigma_s = 0.06$ according to a Monte Carlo and Gauss von Mises simulation. Results are presented at three different propagation times (after 1 day, 5 days, and 10 days of maneuvers.)
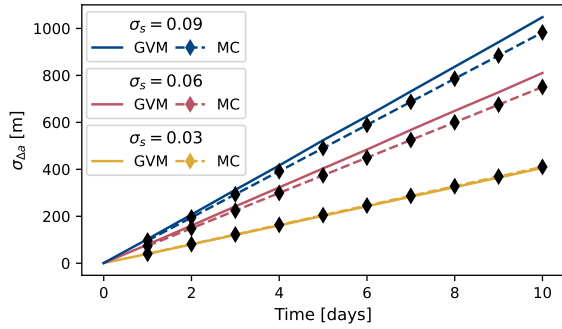

Figure 6: Evolution in time of the standard deviation of the increase in semi-major axis for three different specularity standard deviations, σ_s. Data was obtained through Monte Carlo and Gauss von Mises simulations.

Figure 6 confirms that growth of the standard deviation of the SMA gain is linear in time; if the standard deviation after 1 day of maneuvers is 100 m, for instance, then one could expect a standard deviation of 1 km after 10 days of maneuvers. As shown in the figure, the slope of these trends is driven by the standard deviation of the input uncertainty, the specularity. Higher input uncertainties lead to faster growing SMA uncertainties. This figure also shows how the GVM method tends to overestimate the output standard deviation, an effect that is more pronounced the greater the input standard deviation is.

4.2.3. Uncertainty due to coupled uncertainties

Sections 4.2.1 and 4.2.2 have dealt with the effects of individual input uncertainties on the uncertainty of the SMA increase. This section discusses the effects of multiple input uncertainties simultaneously on this same figure of merit. The results appear in Figure 7.
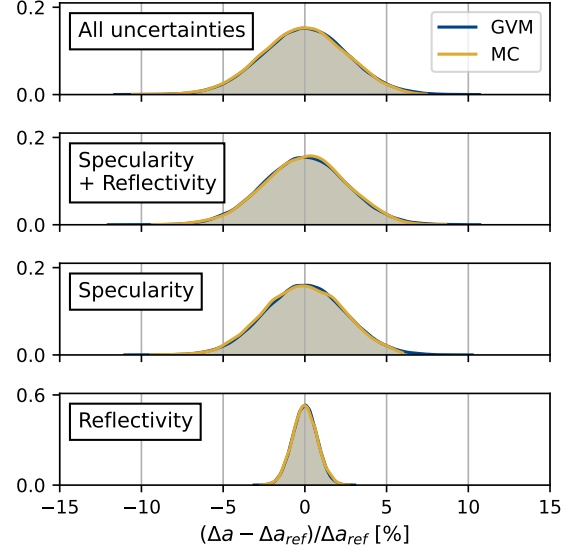

Figure 7: Distribution of the semi-major axis increase after 10 days of maneuvers according to Monte Carlo and Gauss von Mises simulations. Results are presented for different sets of input uncertainties.

Four sets of uncertainties are considered: all uncertainties shown in Table 1, only specularity and reflectivity, only specularity, and only reflectivity. All input uncertainties are normally distributed with standard deviations as shown in column σ_1 of Table 1. As seen in the figure, the distribution for "Specuality + Reflectivity" largely resembles the distribution when considering all uncertainties. Moreover, once again, the results from the Gauss von Mises method seem to agree with those of the Monte Carlo simulations.

Table 3: Standard deviation of the distributions shown in Fig. 7.

| | $\sigma_{\Delta a}/\Delta a_{\text{ref}}$ [%] | |
	GVM	MC
All uncertainties	2.644	2.575
Specularity + Reflectivity	2.586	2.518
Specularity	2.471	2.408
Reflectivity	0.759	0.761

Table 3 provides further insight into the spread of the distributions for the four sets of input uncertainties. As expected, the standard deviation is larger the more uncertain parameters are considered. However, this table also shows that the specularity and reflectivity are very clearly dominant, with other uncertainties being essentially negligible. This demonstrates that analysis effort might be saved if the most dominant input uncertain-

ties (or, alternatively, the negligible ones) are identified early on.

It is important to highlight that these results indicate a 7.5% 3σ uncertainty in SMA gain due to the optical coefficient uncertainties in the NEA Scout solar-sail model. For instance, if the nominal SMA increase were 10 km, this would translate to a 3σ uncertainty of 750 m in the SMA increase. Such uncertainty could potentially have a significant and detrimental effect on mission performance.

4.3. Stochastic process uncertainties

Previous sections dealt with constant random value uncertainties, where certain input parameters, such as the reflectivity or the billow of the sail, were random but fixed during propagation. This section shows results for the uncertainty caused by considering a randomly evolving offset on the nominal attitude profile.
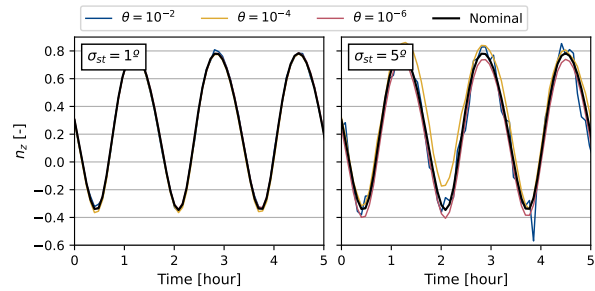

Figure 8: Evolution of the z component of the sail normal direction in the J2000 Earth-centered inertial reference frame for different values of σ_{st} and θ for the first hours of propagation of the test case. The "Nominal" line indicates the locally optimal direction (without random offset).

To gain insights into the impact of the Ornstein-Uhlenbeck parameters θ and σ_{st} (see Section 3.2) on the sail's attitude, refer to Figure 8. This figure illustrates the evolution of the z component of the sail normal direction for six different combinations of the Ornstein-Uhlenbeck parameters. By comparing these examples with the nominal evolution for this parameter, one can better understand the influence of θ and σ_{st} on the sail's behavior.

The effect of the stationary standard deviation σ_{st} is relatively easy to understand: higher values of this parameter mean that the offset direction will generally be further away from the reference direction. The θ parameter, on the other hand, influences how "fast" the offset changes. As seen for the lines corresponding to $\theta = 10^{-2}$, the behaviour is clearly "noisy", with the offset rapidly moving above and below the reference. Instead, for $\theta = 10^{-6}$, the offset evolves so slowly that it seems constant during the 10-hour window plotted in

Fig. 8. The line for $\theta = 10^{-4}$ represents a middle point: it is not as "noisy", but one can see it move with respect to the reference.
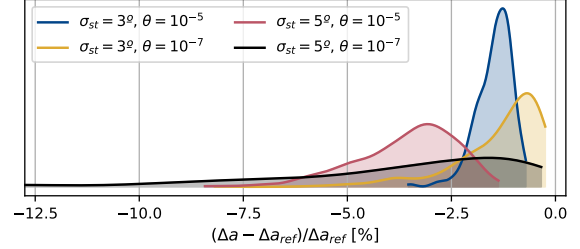

Figure 9: Distribution of the semi-major axis increase after 10 days of maneuvers for different Ornstein-Uhlenbeck parameters θ and σ_{st}.

Figure 9 shows how different values of the Ornstein-Uhlenbeck parameters θ and σ_{st} affect both the mean and standard deviation of the output distributions. This is in contrast to previous analysis showcased in this paper, where the mean of the distribution always remained equal to the nominal performance. As such, this section discusses the behaviour of both the mean $\mu_{\Delta a}$ and standard deviation $\sigma_{\Delta a}$ as a function of the Ornstein-Uhlenbeck parameters θ and σ_{st}.
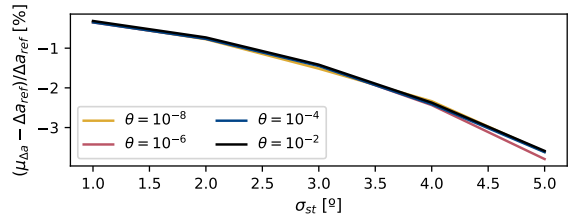

Figure 10: Mean semi-major axis increase after 10 days of maneuvers as a function of the Ornstein-Uhlenbeck parameter σ_{st} for different values of θ.

Figure 10 reveals the strong relationship between the stationary standard deviation σ_{st} and the mean gain in SMA $\mu_{\Delta a}$. In contrast, the parameter θ seems to have a negligible effect on this metric. As such, mean performance loss due to uncertain attitude is mainly driven by the stationary standard deviation of the attitude with respect to the optimal control profile. Note that for all cases studied, the mean performance was below the nominal performance $\mu_{\Delta a} < \Delta a_{ref}$. This indicates that neglecting to model attitude uncertainty will always lead to overestimated performance expectations.

On the other hand, Fig. 11 shows that both parameters θ and σ_{st} affect the spread of the SMA gain distribution. Perhaps unsurprisingly, higher values of the standard deviation of the attitude uncertainty σ_{st} lead to
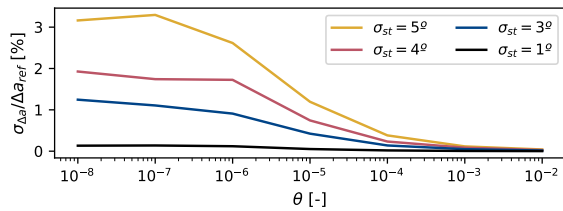
Figure 11: Standard deviation of the semi-major axis increase after 10 days of maneuvers as a function of the Ornstein-Uhlenbeck parameter θ for different values of $\sigma_{\rm st}$.

higher values of the standard deviation of the figure of merit $\sigma_{\Delta a}$.

In contrast, when considering smaller values of θ, there is a notable increase in the standard deviation of the relative SMA gain. These smaller values of θ correspond to attitude offsets that evolve at a significantly slower pace, eventually reaching a point where they remain relatively constant for extremely small values of θ. Consequently, the attitude profiles across different propagations exhibit substantial dissimilarities, resulting in a higher standard deviation in the relative SMA gain. Conversely, higher values of θ yield rapidly changing attitude offsets. As a result, individual propagations exhibit comparable attitude profiles, leading to a reduced standard deviation in the relative increase of SMA.

5. Conclusion

In conclusion, this paper has shed light on the significance of uncertainty in solar-sail mission design. The findings underscore the substantial impact of uncertainty in optical coefficients on mission performance, as demonstrated by the NEA Scout's sail coefficients, which resulted in a notable 3-σ mission performance uncertainty of 7.5%. Notably, specularity uncertainty played a the largest role in this performance uncertainty.

Furthermore, the study on attitude uncertainty revealed not only its impact on mission performance uncertainty, but also highlighted that assuming an ideal control profile may lead to overestimated performance expectations. By incorporating the Ornstein-Uhlenbeck process with tunable parameters, different types of noise in attitude profiles were modeled, resulting in performance distributions with different means and spread.

The Gauss von Mises method proved to be an efficient and effective uncertainty propagation technique, demonstrating its capability at the benefit of a considerably lower computational cost compared to Monte Carlo simulations.

Future research will expand upon the analysis presented in this study by considering different test cases.

This includes exploring other initial orbits, such as orbits with shadowing effects, as well as investigating alternative control strategies, such as inclination change maneuvers. Such endeavors will further enhance our understanding of uncertainty in solar-sail mission design and contribute to the development of more robust and reliable mission planning strategies.

References

[1] Colin McInnes. Solar Sailing Technology, Dynamics and Mission Applications. Technical report, 1999.

[2] Tomohiro YAMAGUCHI et al. Trajectory Analysis of Small Solar Sail Demonstration Spacecraft IKAROS Considering the Uncertainty of Solar Radiation Pressure. *TRANSACTIONS OF THE JAPAN SOCIETY FOR AERONAUTICAL AND SPACE SCIENCES, AEROSPACE TECHNOLOGY JAPAN*, 8, 2010. ISSN 1884-0485.

[3] Ofer Eldad, E. Glenn Lightsey, and Christian Claudel. Minimum-time attitude control of deformable solar sails with model uncertainty. *Journal of Spacecraft and Rockets*, 54(4):863–870, 6 2017. ISSN 15336794.

[4] Lorenzo Niccolai et al. Effects of optical parameter measurement uncertainties and solar irradiance fluctuations on solar sailing. *Advances in Space Research*, 67(9):2784–2794, 5 2021. ISSN 18791948.

[5] Kenshiro Oguri, Gregory Lantoine, and Theodore H Sweetser. Robust Solar Sail Trajectory Design under Uncertainty with Application to NEA Scout Mission. Technical report, 2021.

[6] Andrew Heaton, Naeem Ahmad, and Kyle Miller. Near Earth Asteroid Scout Thrust and Torque Model. In *The 4th International Symposium on Solar Sailing*, 2017.

[7] Justin R. Mansell et al. Orbit and attitude performance of the lightsail 2 solar sail spacecraft. *AIAA Scitech 2020 Forum*, 2020. doi: 10.2514/6.2020-2177.

[8] Joshua T. Horwood and Aubrey B. Poore. Gauss von Mises distribution for improved uncertainty realism in space situational awareness. *SIAM-ASA Journal on Uncertainty Quantification*, 2(1), 2014. ISSN 21662525.

[9] G. E. Uhlenbeck and L. S. Ornstein. On the Theory of the Brownian Motion. *Physical Review*, 36(5):823, 9 1930. ISSN 0031899X.

[10] W. Keats Wilkie et al. An Overview of the NASA Advanced Composite Solar Sail (ACS3) Technology Demonstration Project. 2021.

[11] Karel F Wakker. *FUNDAMENTALS OF ASTRODYNAMICS*. 2015. ISBN 9789461864192. URL http://repository.tudelft.nl.

[12] B. Tapley et al. The GGM03 Mean Earth Gravity Model from GRACE. *AGUFM*, 2007.

[13] L. Rios-Reyes and D. J. Scheeres. Trajectory control for general solar sails. In *AIAA Guidance, Navigation and Control Conference and Exhibit*. American Institute of Aeronautics and Astronautics Inc., 2008. ISBN 9781563479458. doi: 10.2514/6.2008-6830.

[14] Livio Carzana, Pieter Visser, and Jeannette Heiligers. A New Model for the Planetary Radiation Pressure Acceleration for Solar Sails. 2022.

[15] Giovanni Mengali and Alessandro A. Quarta. Near-optimal solar-sail orbit-raising from low earth orbit. *Journal of Spacecraft and Rockets*, 42(5):954–958, 2005. ISSN 15336794. doi: 10.2514/1.14184.

[16] Joel A. Storch. Aerodynamic Disturbances on Rapidly Rotating Spacecraft in Free-Molecular Flow. In *Engineering Construction and Operations in Challenging Environments Earth and Space 2004: Proceedings of the Ninth Biennial ASCE Aerospace Division International Conference*, pages 429–436. American Society of Civil Engineers (ASCE), 2004. ISBN 0784407223. doi: 10.1061/40722(153)60.

[17] Malcolm MacDonald and Colin R McInnes. Realistic Earth Escape Strategies for Solar Sailing. *JOURNAL OF GUIDANCE, CONTROL, AND DYNAMICS*, 28(2), 4 2005. doi: 10.2514/1.5165.

[18] Malcolm MacDonald and Colin R McInnes. Analytical Control Laws for Planet-Centered Solar Sailing. *JOURNAL OF GUIDANCE, CONTROL, AND DYNAMICS*, 28(5), 10 2005. doi: 10.2514/1.11400.

[19] Kristian Debrabant. Runge-Kutta methods for third order weak approximation of SDEs with multidimensional additive noise. 2010.

[20] G Greschik and M M Mikulas. Design Study of a Square Solar Sail Architecture. *JOURNAL OF SPACECRAFT AND ROCKETS*, 39(5), 2002. doi: 10.2514/2.3886.